

Journal Pre-proofs

Research paper

Syntheses, spectroscopy, tautomerism, induced chirality and molecular structure of 3-(*o/p*-tolylimino)indolin-2-one and *bis*[3-(*o/p*-tolylimino)indole-2-olato- κ^2 N,O]- Δ/Λ -zinc(II)

Mohammed Enamullah, Mohammad Khairul Islam, Simon-Patrick Höfert, Christoph Janiak

PII: S0020-1693(19)31457-4
DOI: <https://doi.org/10.1016/j.ica.2019.119245>
Reference: ICA 119245

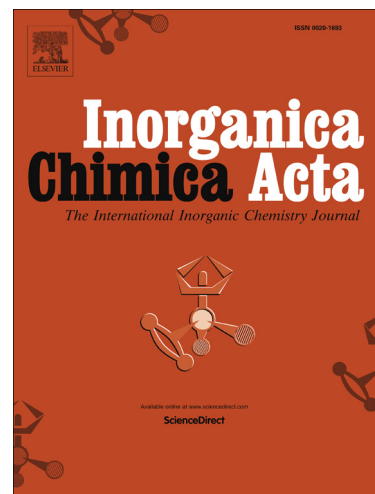
To appear in: *Inorganica Chimica Acta*

Received Date: 21 September 2019
Revised Date: 29 October 2019
Accepted Date: 31 October 2019

Please cite this article as: M. Enamullah, M.K. Islam, S-P. Höfert, C. Janiak, Syntheses, spectroscopy, tautomerism, induced chirality and molecular structure of 3-(*o/p*-tolylimino)indolin-2-one and *bis*[3-(*o/p*-tolylimino)indole-2-olato- κ^2 N,O]- Δ/Λ -zinc(II), *Inorganica Chimica Acta* (2019), doi: <https://doi.org/10.1016/j.ica.2019.119245>

This is a PDF file of an article that has undergone enhancements after acceptance, such as the addition of a cover page and metadata, and formatting for readability, but it is not yet the definitive version of record. This version will undergo additional copyediting, typesetting and review before it is published in its final form, but we are providing this version to give early visibility of the article. Please note that, during the production process, errors may be discovered which could affect the content, and all legal disclaimers that apply to the journal pertain.

© 2019 Elsevier B.V. All rights reserved.



Syntheses, spectroscopy, tautomerism, induced chirality and molecular structure of 3-(*o/p*-tolylimino)indolin-2-one and bis[3-(*o/p*-tolylimino)indole-2-olato- κ^2 N,O]- Δ/Λ -zinc(II)

Mohammed Enamullah ^{a,*}, Mohammad Khairul Islam, Simon-Patrick Höfert, Christoph Janiak ^b

^a *Department of Chemistry, Jahangirnagar University, Dhaka-1342, Bangladesh. E-mail: enamullah@juniv.edu*

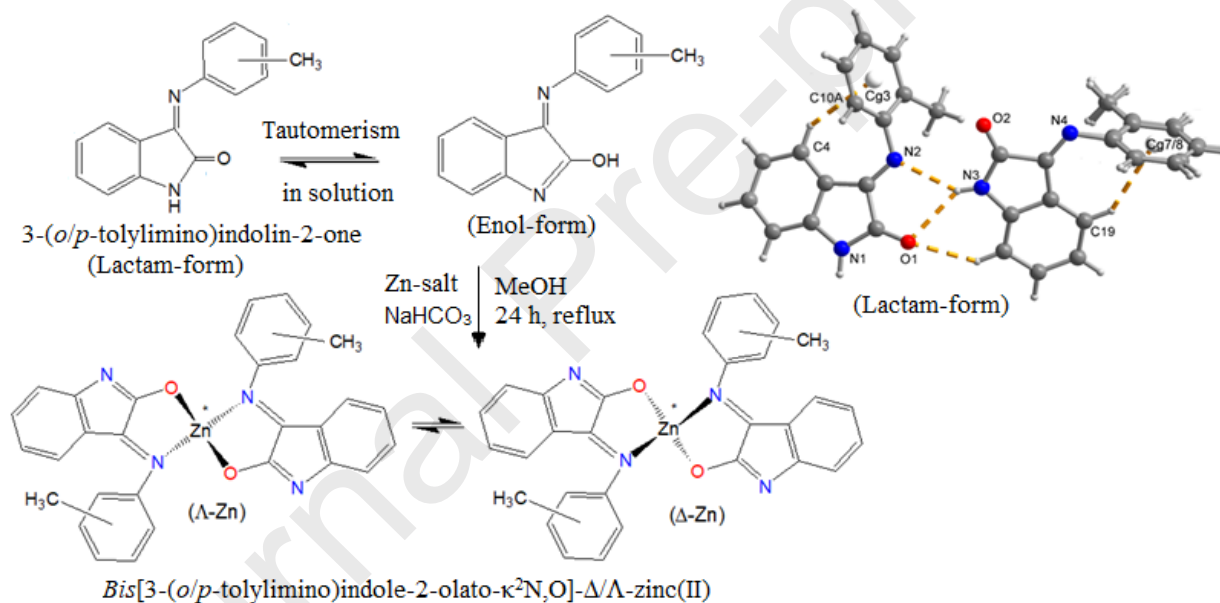
^b *Institut für Anorganische Chemie und Strukturchemie, Heinrich-Heine-Universität, Universitätsstr. 1, D-40225 Düsseldorf, Germany.*

Graphical Abstract

Syntheses, spectroscopy, tautomerism, induced chirality and molecular structure of 3-(*o/p*-tolylimino)indolin-2-one and *bis*[3-(*o/p*-tolylimino)indole-2-olato- κ^2 N,O]- Δ/Λ -zinc(II)

Mohammed Enamullah ^{a,*}, Mohammad Khairul Islam, Simon-Patrick Höfert and Christoph Janiak ^b

Isatin-Schiff bases 3-(*o/p*-tolylimino)indolin-2-one undergo tautomerism between the lactam (L)- and enol (E)-forms in solution, which in turn reacts with zinc(II) nitrate to give *bis*[3-(*o/p*-tolylimino)indole-2-olato- κ^2 N,O]- Δ/Λ -zinc(II) (**1** and **2**).



Highlights

- *Bis*[3-(*o/p*-tolylimino)indole-2-olato- κ^2 N,O]- Δ/Λ -zinc(II)
- Induced chirality (Δ and Λ) at-metal center
- Lactam-Enol tautomerism
- Hirshfeld surfaces analyses
- DFT/TDDFT calculations

Abstract

The isatin-Schiff bases 3-(*o/p*-tolylimino)indolin-2-one (HL1 and HL2) undergo tautomerization from lactam (L)- to enol (E)-form in solution, which in turn reacts with zinc(II) nitrate to give *bis*[3-(*o/p*-tolylimino)indole-2-olato- κ^2 N,O]- Δ/Λ -zinc(II) (**1** and **2**). IR spectra for the Schiff bases suggest solely the lactam-form at solid state, while both the forms in solution. ^1H NMR spectra show the peaks associated to both the lactam- and enol-forms in solution. Molecular structure for HL1 explores two symmetry independent molecules (A and B) in an asymmetric unit due to intermolecular O \cdots H and N \cdots H hydrogen bonding interactions. The molecule crystallises with monoclinic $P2_1/n$ space group. Supramolecular analyses suggest that the packing in the crystals is organized, in addition to hydrogen bonds, by a few *intra*- and *inter*-molecular C-H $\cdots\pi$ contacts. Studies of Hirshfeld surfaces using CrystalExplorer strongly support the quantitative analyses by supramolecular packing in the crystals. ^1H NMR spectra for **1** or **2** show two sets of peaks for each proton, correspond to the Δ -Zn and Λ -Zn configured isomers at a ratio of *ca.* 65:35, resulting from induced chirality at-metal centre. ^1H NMR spectra taken at different time intervals rule out any possibility of interconversion between the isomers in solution, that is, the same ratio of the isomers exists at solid state. These results indicate preferential formation one isomer over another (i.e., Δ -Zn or Λ -Zn) both in solution and at solid state. Optimized structures and excited state properties by DFT/TDDFT correspond well to the experimental spectra.

Keywords: Induced chirality (Δ vs. Λ); Δ -Zn and Λ -Zn isomers; Zinc(II)-isatin Schiff bases; Lactam- and Enol-tautomerism; DFT/TDDFT.

1. Introduction

The transition metal(II)-complexes with *chiral/achiral*-asymmetric bidentate ligands in tetrahedral to distorted square-planar geometry exhibit induced chirality at-metal center and provide the right (Δ)- and left (Λ)-handed configured isomers (i.e., opposite configuration at metal) along the C_2 -symmetry of the molecule [1-2]. Use of an *achiral* ligand $A^{\wedge}B$ gives the

isomers of non-planar Δ -M(A[^]B)₂ and Λ -M(A[^]B)₂ configured complexes. The enantiopure ligands (*R* or *S*-A[^]B) provide the diastereomeric pairs of Δ -M(*R*-A[^]B)₂ and Λ -M(*R*-A[^]B)₂ {or Λ -M(*S*-A[^]B)₂ and Δ -M(*S*-A[^]B)₂}, while the racemic ligands (*R/S*-A[^]B) gives all four diastereomers. It has well been documented that the non-covalent interactions acting within the metal-ligands co-ordination sphere lead to a free energy difference between the Δ -M and Λ -M isomers and hence one of the isomers is thermodynamically and/or kinetically preferred [3-13]. The phenomenon can efficiently control by ligand design and/or chirality, metal ion selection and solute-solvent interactions, respectively [3-13]. In addition, the *inter*- and *intra*-molecular interactions such as hydrogen bonds, $\pi \dots \pi$ and C–H... π contacts in the crystal packing direct the induced chirality very selective way and provide the Δ -M and/or Λ -M isomers [9,13].

We have investigated the phenomenon in details using the four-coordinated, non-planar and C₂-symmetric transition metal(II)-complexes with *chiral* Schiff bases ligands, [M(*R*- or *S*-N[^]O)₂] (M = Fe, Co, Ni, Cu, Zn; N[^]O = deprotonated Schiff bases anion = salicylal- or naphthal-diminate) both in solution and at solid state [3-13]. Our results unequivocally demonstrate the preferred formation of the Δ -*R*-M or Λ -*S*-M isomer and *vice versa* (i.e., Δ -*S*-M or Λ -*R*-M) as evidenced by X-ray structural analyses, electronic/vibrational circular dichroism (ECD/VCD), ¹H NMR studies, thermal analyses and DFT/TDDFT calculations, respectively. The solid-state X-ray structures determinations demonstrate that the co-ordination of enantiopure *R* or *S*-ligands (or *racemic R/S*-ligands) to the metal ion diastereoselectively gives the enantiopure crystals with absolute configuration of Λ -*R*-M or Δ -*S*-M (or *racemic* crystals with Λ/Δ -*R/S*-M or Δ/Λ -*R/S*-M configuration) and *vice versa*. Though the induced chirality is quantitative at solid-state, it becomes rather complicated in solution, where a dynamic interconversion equilibrium prevails between Δ -*R*-M and Λ -*R*-M (or Δ -*S*-M and Λ -*S*-M) isomers. Use of *racemic* ligands show an equilibrium between the Λ/Δ -*R/S*-M and Δ/Λ -*R/S*-M isomers and *vice versa*. However, if the equilibrium process is considerably slow, it can easily be followed by running variable time and temperature dependent ¹H NMR spectra for the diamagnetic complexes, respectively. Thus, the equilibrium shifts from a single-isomer of Λ/Δ -*R/S*-M (i.e., 100% within 10 min of complex dissolution) to a ratio of 33:67 (Δ/Λ -*R/S*-M: Λ/Δ -*R/S*-M within 40 min) or 46:54 (within 36 h) for the *racemic* zinc(II)-(*R/S*)-aminoalcohol based Schiff bases complexes [3]. In contrary, similar studies result in no shifts of equilibrium with

time for enantiopure zinc(II)-(*R* or *S*)-naphthaldimine complexes [6]. Indeed, variable temperature (VT) ^1H NMR studies on the later complexes show temperature-dependent shifts of the equilibrium with a ratio of 87:13 (Δ -*S*-*M*: Λ -*S*-*M*) at $-50\text{ }^\circ\text{C}$ to 73:27 at $35\text{ }^\circ\text{C}$ in solution [6]. Indeed, studies of VT electronic circular dichroism (ECD) spectra reveal the parallel results in Co/Zn(II)-(*R* or *S*)-salicylal-/naphthal-dimine complexes in solution [6,11].

We have reported two examples of induced chirality at-metal center, so far, in Zn(II)-complexes with *achiral* Schiff bases ligands, which provide both Δ - and Λ -configured complexes in a single crystals [9,13]. The *achiral* Schiff-bases, *N*-2-(pyridyl)salicylaldimine react with the zinc(II) salts to provide the enantiomorphous *chiral* at-metal centered *bis*[*N*-2-(pyridyl)salicylaldiminato- $\kappa^2\text{N},\text{O}$]- Δ/Λ -zinc(II), which crystallizes as a racemic conglomerate *via* spontaneous resolution [9]. The Δ - and Λ -configured complexes assemble in *P* (right)- and *M* (left)-handed 4_1 - and 4_3 -helical chains *via* weak intermolecular C–H \cdots O hydrogen bonds. Further, only the same Δ - or Λ -configured molecules are combined into a helical chain, and only the chains of the same *P*- or *M*-handedness are combined with the corrugated van-der-Waals surfaces through weak interactions to form the homochiral crystals [9]. Another example of induced Δ - and Λ -chirality is reported in *bis*[*N*-2-(*R*-pyridyl)-2-oxo-1-naphthaldiminato- $\kappa^2\text{N},\text{O}$]- Λ - and Δ -zinc(II), (*R* = H, 4/6- CH_3) by *achiral* Schiff bases ligands [13]. The supramolecular packing analysis exhibit strong π - π interactions resulting an inversion-symmetric complexes pair with opposite Λ - and Δ -configurations at-metal center.

In view of further investigations along induced Δ - and Λ -chirality, we have synthesized the isatin-Schiff bases and their complexes with transition metal ions [14,15]. The isatin-Schiff bases readily react with the copper(II) ion to give the *bis*[3-(*o/p*-tolylimino)indole-2-olato- $\kappa^2\text{N},\text{O}$]copper(II) [15]. Similar reaction with the dinuclear $[\text{Rh}(\mu\text{-O}_2\text{CMe})(\eta^4\text{-cod})]_2$ (*cod* = 1,5-cyclooctadiene) provides the mononuclear $[\text{Rh}(\eta^4\text{-cod})\{3\text{-}((R)\text{-}(\text{Ar})\text{-ethylimino})\text{-}3H\text{-indol-}2\text{-olato}\}]$ [14]. The present endeavor, in continuation, reports the results of syntheses, spectroscopy, tautomerism, induced chirality and X-ray molecular structure of the isatin-Schiff bases 3-(*o/p*-tolylimino)indolin-2-one (HL1 and HL2) and *bis*[3-(*o/p*-tolylimino)indole-2-olato- $\kappa^2\text{N},\text{O}$]- Δ/Λ -zinc(II) (**1** and **2**), respectively. The optimized structures and excited state properties by DFT/TDDFT are employed to get detailed insights into experimental results.

2. Experimental

2.1. Materials and measurements

UV-Vis. spectra were obtained with the Shimadzu UV 1800 spectrophotometer in methanol at 25 °C. Nicolet iS10 (Thermo Scientific) spectrometer was used to run IR spectra at solid state (KBr discs) and in CHCl₃ at ambient temperature. Elemental analyses were performed on a VarioEL from the Elementaranalysensysteme. ¹H NMR-spectra were recorded on Bruker Avance 400 spectrometer operating at 400 MHz in CDCl₃ at 20 °C.

2.2. Syntheses of the Schiff bases (HL1 and HL2)

An equimolar amount of indoline-2,3-dione (isatin) and *o/p*-toluidine were dissolved in 10 mL methanol. Three drops of concentrated H₂SO₄ was added into this mixture solution, which was then refluxed for 6-8 hours. Colour of the solution changed to orange-yellow. Afterwards, reduced the volume of the solution to *ca.* 50% in *vacuo* and left standing the solution for crystallization *via.* slow evaporation of solvent at room temperature. Orange-yellow micro crystals were formed after 2-3 days, filtered off and washed the crystals with methanol (2 ml in each) for three times. Dried the product in air for 3-4 days and obtained micro crystals of the Schiff bases, 3-(*o/p*-tolylimino)indolin-2-one (HL1 and HL2). X-ray quality single crystals for HL1 are obtained by slow evaporation of concentrated methanol solution after 4-5 days.

2.2.1. 3-(*o*-tolylimino)indolin-2-one (HL1):

Yield: 8.520 g (82%). IR (KBr, cm⁻¹): 3454br (νH₂O), 3259s (νN-H), 3184, 3087, 2914w (νC-H), 1742, 1724vs (νC=O) and 1613, 1593vs (νC=N). IR (CHCl₃, cm⁻¹): 3693, 3683, 3609w (νO-H), 3439s (νN-H), 1746s, 1734sh (νC=O) and 1619s, 1603sh (νC=N). IR (ATR, cm⁻¹): 3234w (νN-H), 3066w (νC-H), 1744, 1717vs (νC=O) and 1610, 1593vs (νC=N). ¹H NMR (400 MHz, CDCl₃): δ = 2.18 (s, 3H, CH₃-L, 93%), 2.38 (s, 3H, CH₃-E, 17%), 6.52 (d, *J* = 7.6 Hz, 1H, H₁₄-L), 6.67 (t, *J* = 7.6 Hz, 1H, H₁₃-L), 6.87 (d, *J* = 7.6 Hz, 1H, H₁₁-L), 6.97 (d, *J* = 7.8 Hz, 1H, H₈-L), 7.00 (m, 1H, H₁₄-E), 7.15 (m, 2H, H_{11,13}-E), 7.19 (t, *J* = 7.2 Hz, 1H, H₁₂-L), 7.27 (t, *J* = 7.2 Hz, 1H, H₆-L), 7.32 (d, *J* = 7.6 Hz, 2H, H_{6,12}-E+2H, H_{5,7}-L), 7.33 (d, *J* = 7.5 Hz, 1H, H₈-E), 7.56 (t, *J* = 7.6 Hz, 1H, H₇-E), 7.62 (d, *J* = 7.5 Hz, 1H, H₅-E), 9.35 (br, 1H, OH-E, 8%), 9.62 (br, 1H, NH-L, 92%) (L/E= lactum-/enol-form; for proton numbering see the Scheme 1).

2.2.2. 3-(*p*-tolylimino)indolin-2-one (HL2):

Yield 9.10 g (83%). IR (KBr, cm^{-1}): 3451br ($\nu\text{H}_2\text{O}$), 3241s ($\nu\text{N-H}$), 3067s, 2920w ($\nu\text{C-H}$), 1748vs, 1720s ($\nu\text{C=O}$) and 1612vs, 1594sh ($\nu\text{C=N}$). IR (CHCl_3 , cm^{-1}): 3689, 3676, 3610w ($\nu\text{O-H}$), 3439s ($\nu\text{N-H}$), 1745s ($\nu\text{C=O}$) and 1616s, 1595sh ($\nu\text{C=N}$). IR (ATR, cm^{-1}): 3252w ($\nu\text{N-H}$), 3167, 3022w ($\nu\text{C-H}$), 1740, 1722vs ($\nu\text{C=O}$) and 1609, 1591vs ($\nu\text{C=N}$). ^1H NMR (400 MHz, CDCl_3): δ = 2.28 (s, 3H, $\text{CH}_3\text{-E}$, *ca.* 15%), 2.43 (s, 3H, $\text{CH}_3\text{-L}$, *ca.* 85%), 6.79 (t, J = 7.6 Hz, 1H, $H_6\text{-L}$), 6.83 (t, J = 7.2 Hz, 1H, $H_5\text{-L}$), 6.95 (d, J = 8.0 Hz, 1H, $H_8\text{-L}$), 6.98 (d, J = 8.0 Hz, 4H, $H_{11-12,14-15}\text{-L}$), 7.06 (m, 1H, $H_8\text{-E}$), 7.13 (t, J = 7.6 Hz, 1H, $H_6\text{-E}$), 7.26 (d, J = 8.0 Hz, 4H, $H_{11-12,14-15}\text{-E}$), 7.33 (t, J = 7.2 Hz, 1H, $H_7\text{-L}$), 7.57 (t, J = 7.6 Hz, 1H, $H_7\text{-E}$), 7.63 (d, J = 7.6 Hz, 1H, $H_5\text{-E}$), 8.91 (br, 1H, OH-E, 18%) and 9.19 (br, 1H, NH-L, 82%).

2.3. Syntheses of the complexes (1 and 2)

Two equivalents of isatin-Schiff base 3-(*o/p*-tolylimino)indolin-2-one (HL1 or HL2) (0.236 g, 1 mmol) were dissolved in 10 ml of methanol and stirred the solution for 10 min. Added one equivalent of Zn(II) nitrate (0.131 g, 0.5 mmol), dissolved in 10 mL methanol, into this solution. Afterwards, two equivalents of NaHCO_3 (dissolved in 5 ml methanol) poured into the mixture solution and refluxed the solution. An orange-yellow precipitate was started in the solution with 2-3 hours of reflux. After 24 hours reflux, cooled the reaction mixture to room temperature, and left standing this solution for complete precipitation. Filtered off the precipitate and washed two times with methanol (2 mL in each) followed by diethyl ether (2 mL in each), respectively. The orange-yellow micro crystals of bis[3-(*o/p*-tolylimino)indole-2-olato- $\kappa^2\text{N,O}$]zinc(II) (**1** or **2**) were obtained after drying the products in oven at 40 °C for 24 hours.

2.3.1. Bis[3-(*o*-tolylimino)indole-2-olato- $\kappa^2\text{N,O}$]zinc(II), (**1**):

Yield: 0.215 g (73%). IR (KBr, cm^{-1}): 3067, 2923w ($\nu\text{C-H}$), 1733s ($\nu\text{C=O}$) and 1633, 1593, 1584vs ($\nu\text{C=N}$). IR (ATR, cm^{-1}): 3065, 2930w ($\nu\text{C-H}$), 1734s ($\nu\text{C=O}$) and 1634, 1591vs ($\nu\text{C=N}$). ^1H NMR (400 MHz, CDCl_3): δ = 2.17 (s, 3H, $\text{CH}_3\text{-}\Delta$, *ca.* 85%), 2.20 (s, 3H, $\text{CH}_3\text{-}\Lambda$, *ca.* 15%), 6.54 (d, J = 8.0 Hz, 1H, $H_{14}\text{-}\Delta$), 6.77 (t, J = 7.6 Hz, 1H, $H_{13}\text{-}\Delta$), 6.86 (d, J = 7.6 Hz, 1H, $H_{11}\text{-}\Delta$), 6.90 (d, J = 8.0 Hz, 1H, $H_8\text{-}\Delta$), 6.91 (d, J = 8.0 Hz, 1H, $H_{14}\text{-}\Lambda$), 7.17 (m, 1H, $H_{11}\text{-}\Lambda$), 7.18 (t, J = 7.2 Hz, 1H, $H_{12}\text{-}\Delta$), 7.26 (t, J = 7.6 Hz, 1H, $H_6\text{-}\Delta$), 7.28-7.32 (m, 4H, $H_7\text{-}\Delta$, $H_{6,12,13}\text{-}\Lambda$), 7.35 (d, J = 7.6 Hz, 1H, $H_8\text{-}\Lambda$),

7.59 (t, $J = 7.6$ Hz, 1H, $H_{7-\Delta}$), 7.65 (d, $J = 7.6$ Hz, 1H, $H_{5-\Delta}$), 7.83 (br, 1H, $H_{5-\Delta}$) (for proton numbering see the Scheme 1). – $C_{30}H_{22}N_4O_2Zn \cdot 3H_2O$ (589.96): Calcd C 61.08, H 4.78, N 9.50; found C 60.80, H 4.60, N 9.30.

2.3.2. *Bis[3-(p-tolylimino)indole-2-olato- κ^2N,O]zinc(II), (2)}*:

Yield 0.210 g (71%). IR (KBr, cm^{-1}): 3058, 2923w (vC-H), 1735s (vC=O) and 1637, 1594, 1580vs (vC=N). 1H NMR (400 MHz, $CDCl_3$): $\delta = 2.31$ (s, 3H, $CH_3-\Lambda$, 45%), 2.43 (s, 3H, $CH_3-\Delta$, ca. 55%), 6.26 (m, 2H, $H_{11,15-\Lambda}$), 6.79 (t, $J = 7.6$ Hz, 1H, $H_{11-\Delta}$), 6.83 (t, $J = 7.6$ Hz, 1H, $H_{15-\Delta}$), 6.91 (t, $J = 7.6$ Hz, 1H, $H_{6-\Delta}$), 6.97 (d, $J = 8.0$ Hz, 2H, $H_{12,14-\Delta}$), 7.11 (t, $J = 7.6$ Hz, 1H, $H_{6-\Delta}$), 7.14 (t, $J = 7.6$ Hz, 1H, $H_{7-\Delta}$), 7.26 (d, $J = 8.0$ Hz, 2H, $H_{12,14-\Lambda}$), 7.33 (t, $J = 7.6$ Hz, 1H, $H_{7-\Delta}$), 7.58 (m, 1H, $H_{8-\Lambda}$), 7.64 (d, $J = 7.6$ Hz, 1H, $H_{5-\Lambda}$), 7.87 (d, $J = 8.0$ Hz, 1H, $H_{8-\Delta}$), 7.99 (br, 1H, $H_{5-\Delta}$) (for proton numbering see the Scheme 1). – $C_{30}H_{22}N_4O_2Zn \cdot 3H_2O$ (589.96): Calcd C 61.08, H 4.78, N 9.50; found C 60.70, H 4.67, N 9.25.

2.4. *Single crystal X-ray diffraction*

Single crystal of HL1 was carefully selected under a polarizing microscope and mounted on a loop. *Data collection*: Bruker APEX II CCD diffractometer with graphite- or multi-layer mirror mono-chromated Mo- K_α radiation ($\lambda = 0.71073$ Å). Data collection and cell refinement with APEX2 [16] data reduction with SAINT (Bruker) [17]. *Structure analysis and refinement*: The structure was solved by direct methods (SHELXS-97) [18]; refinement was done by full-matrix least squares on F^2 using the SHELXL-97 program suite, empirical (multi-scan) absorption correction with SADABS (Bruker) [19]. All non-hydrogen positions were refined with anisotropic temperature factors. The hydrogen atoms for aromatic CH were positioned geometrically (C–H = 0.95 Å) and refined using a riding model (AFIX 43) with $U_{iso}(H) = 1.2U_{eq}$. The hydrogen atoms for CH_3 were positioned geometrically (C–H = 0.98 Å) and refined using a riding model (AFIX 137) with $U_{iso}(H) = 1.5U_{eq}$. The hydrogen atoms for N-H were found and refined free with $U_{iso}(H) = 1.5U_{eq}$. The tolyl rings are disordered over two positions with about equal occupancy. The carbon atoms of these disordered tolyl rings have only been refined isotropically. Details of X-ray data and refinements are listed in Table 1. Graphics were drawn with the DIAMOND (Version 4.4) [20]. The structural data have been deposited with the

Cambridge Crystallographic Data Center (CCDC-numbers 1922815). These data can be obtained free of charge via www.ccdc.cam.ac.uk/data_request/cif.

Table 1. Crystal data and structure refinement for **HL1**.

Empirical formula	C ₁₅ H ₁₂ N ₂ O
M (g mol ⁻¹)	236.27
Crystal size (mm)	0.23 × 0.23 × 0.23
Temperature (K)	140
θ range (°)	1.6 to 27.7
h; k; l range	±19; ±12; -21, +22
Crystal system	monoclinic
Space group	<i>P</i> 2 ₁ / <i>n</i> (14)
a, b, c (Å)	15.1636(14), 9.9282(9), 16.9957(15)
β (deg.)	107.400(4)
<i>V</i> (Å ³)	2441.6(4)
<i>Z</i>	8
<i>D</i> _{calc} [g/cm ⁻³]	1.285
<i>F</i> (000)/ μ (mm ⁻¹)	992/0.082
Trans. (max/min)	1.000/0.845
Reflect. collected, <i>R</i> (int)	18751, 0.037
Independent reflections	5628
Obs. reflections [<i>I</i> > 2 σ (<i>I</i>)]	4108
Data / restraints / parameters	5628/0/323
Largest diff. peak and hole ($\Delta\rho$ /e Å ⁻³)	0.37/-0.23
<i>R</i> ₁ / <i>wR</i> ₂ [<i>I</i> > 2 σ (<i>I</i>)] ^a	0.0538/0.1352
<i>R</i> ₁ / <i>wR</i> ₂ (all reflect.) ^a	0.0785/0.1515
Goodness-of-fit on <i>F</i> ² ^b	1.026

$$-^a R_1 = [\sum (\|F_o| - |F_c|) / \sum |F_o|]; wR_2 = [\sum [w(F_o^2 - F_c^2)^2] / \sum [w(F_o^2)^2]]^{1/2}.$$

$$-^b \text{Goodness-of-fit} = [\sum [w(F_o^2 - F_c^2)^2] / (n-p)]^{1/2}.$$

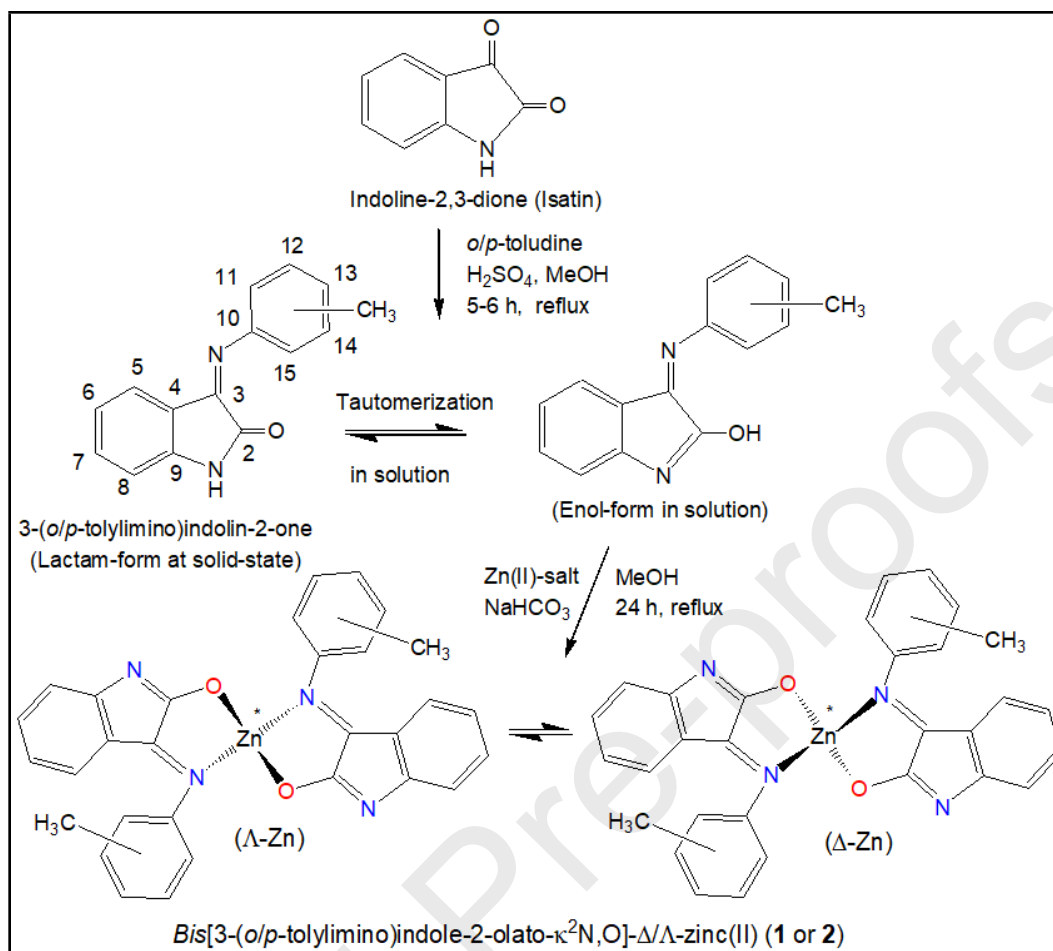
2.5. Computational method

A through computational procedure was performed with the Gaussian 09 software [21] to get further insight and to rationalize the experimental results. As mentioned above, C₂-symmetrical [M(N[^]O)₂] (N[^]O = deprotonated Schiff base anion) complexes with distorted tetrahedral geometry exhibit induced chirality at-metal center and provide the Δ (right)- and Λ (left)-handed

isomers [5-12]. Thus, we optimized two possible isomers having Δ -Zn and Λ -Zn configured structures at B3LYP/6-31G(d) for **1** or **2**, respectively (Fig. 1). The excited state properties by TDDFT were employed with different combinations of the functionals B3LYP, cam-B3LYP and m06, and the basis sets TZVP or SDD on the optimized structures for both the Δ -Zn and Λ -Zn isomers, respectively for **2** [6-7]. Electronic spectra for the Δ -Zn and Λ -Zn isomers for **2** were calculated incorporating Polarization Continuum Model (PCM) using methanol as solvent. 72 excited states (roots) were considered for calculations. A simple and simplified assignments on the excited state properties and molecular orbitals (MOs) calculations were made at the same level of theory. The spectra were generated using the program SpecDis [22] by applying Gaussian band shape with exponential half-width $\sigma = 0.33$ eV.

3. Results and discussion

Reaction of the indoline-2,3-dione (Isatin) with the *o/p*-toluidine under reflux affords the isatin-Schiff bases of 3-(*o/p*-tolylimino)indolin-2-one (HL1 and HL2). The Schiff bases undergo tautomerism between the lactam (L)- and enol (E)-forms in solution, which in turn react with the zinc(II) nitrate in presence of NaHCO_3 under reflux to give the *bis*[3-(*o/p*-tolylimino)indole-2-olato- κ^2 N,O]- Δ/Λ -zinc(II) (**1** or **2**) (Scheme 1).



Scheme 1: Syntheses of the *bis*[3-(*o/p*-tolylimino)indole-2-olato- κ^2 N,O]- Δ/Λ -zinc(II) (1 or 2).

3.1. Vibrational spectra

Vibrational spectra of the isatin-Schiff bases (as KBr disc) show very strong bands at 3259 (HL1)/3241 (HL2) cm^{-1} for ν N-H, and at 1742, 1724 (HL1)/1748, 1720 (HL2) cm^{-1} for ν C=O, correspond to the lactam (L)-form at solid state (Fig. S1) [14-15]. The isatin-Schiff bases undergo tautomerization between the lactam- and enol-forms (Scheme 1) and exhibit bands for both the forms simultaneously in solution [14-15]. To check this, we run the spectra in chloroform solution, which show weak bands at *ca.* 3690, 3610 cm^{-1} (ν O-H) corresponding to the enol-form, while the bands at *ca.* 3439 cm^{-1} (ν N-H) and *ca.* 1743, 1728 cm^{-1} (ν C=O) corresponding to the lactam-form (Fig. S2). The ratio of the bands areas for the lactam to enol forms is *ca.* 3:2, comparable to the ^1H NMR results in solution (discussed below). The spectra further show very strong bands at *ca.* 1612, 1593 cm^{-1} (or *ca.* 1618, 1602 cm^{-1} in CHCl_3) for

$\nu\text{C}=\text{N}$, which shift to *ca.* 1635, 1595 cm^{-1} upon co-ordination to the metal ion in **1** or **2**. The spectra for the complexes (**1** and **2**), taken as KBr disc (Fig. S1), display a strong broad band at *ca.* 3450 cm^{-1} may be due to the $\nu\text{H}_2\text{O}$ (moisture from KBr) or to $\nu\text{N-H}$ and/or $\nu\text{O-H}$ bands from unreacted Schiff bases (if any in the sample). To resolve the issue, we run ATR-IR spectra for the complexes (Fig. S3), which show no bands for the $\nu\text{H}_2\text{O}$, $\nu\text{N-H}$ and/or $\nu\text{O-H}$. The results suggest that there is no free Schiff base in the sample. The spectra further show a weak band at 1734 cm^{-1} for the $\nu\text{C-O}$ and very strong bands at 1634, 1591 cm^{-1} for the $\nu\text{C}=\text{N}$ (Fig. S3). However, since the complexes are formed *via* deprotonation of the enolic-proton (resulting from tautomerism in solution), the $\nu\text{N-H}$ and $\nu\text{O-H}$ (or $\nu\text{C}=\text{O}$) bands are obviously absent in their spectra (Figs. S1 and S3). The ATR spectra for the Schiff bases (Fig. S3) reveal no band for the $\nu\text{H}_2\text{O}$ (as observed in Fig. S1, taken as KBr disc), rather display weak band at *ca.* 3234 (HL1)/3252 (HL2) cm^{-1} for the $\nu\text{N-H}$, while very strong bands at 1744, 1717 (HL1)/1740, 1722 (HL2) cm^{-1} for the $\nu\text{C}=\text{O}$ and at 1610, 1593 (HL1)/1609, 1591 (HL2) cm^{-1} for the $\nu\text{C}=\text{N}$. The overall results of the vibrational spectra strongly indicate the formation of the complexes as depicted in the reaction Scheme 1.

3.2. X-ray molecular structure and packing analyses for HL1:

X-ray molecular structure for HL1 is shown in Fig. 1, and some selected bond lengths and angles are listed in Table 2. The molecule crystallises with monoclinic $P2_1/n$ space group. There are two symmetry independent molecules (A and B) in the asymmetric unit due to the intermolecular hydrogen-bonding interactions (Fig. 1). The molecules A and B differ most significantly in their relative orientations of the aryl- and lactam-rings, which is reflected by the angles between the two planes of the aryl- and lactam-rings ($\theta_1/^\circ$). In molecule A, the two rings are rotated by 69.9/70.0 $^\circ$ (θ_1) with respect to one another, while the two rings are approximately perpendicular to one another with an angle of 88.1/86.5 $^\circ$ (θ_1) in molecule B (Table 2). This difference in orientations arises from the intermolecular hydrogen-bonding interactions and C-H... π contacts in the crystals (Figs. 1 and 2). The values of bond lengths C2-N2/C17-N4 (1.2762/1.2729 Å) indicate the carbon-nitrogen double bond character, while the bond angles C2-N2-C9 (117.74/119.85 $^\circ$) and C17-N4-C24 (119.07/117.58 $^\circ$) represent a sp^2 -hybridization of the imino-nitrogen atom. Indeed, the observed bond lengths and angles are comparable to the optimized structures by DFT (Table 2), and also to the X-ray results for the related *chiral* isatin-

Schiff bases ligands [14]. The X-ray results clearly elucidate the structure of HL1 to be the lactam-form.

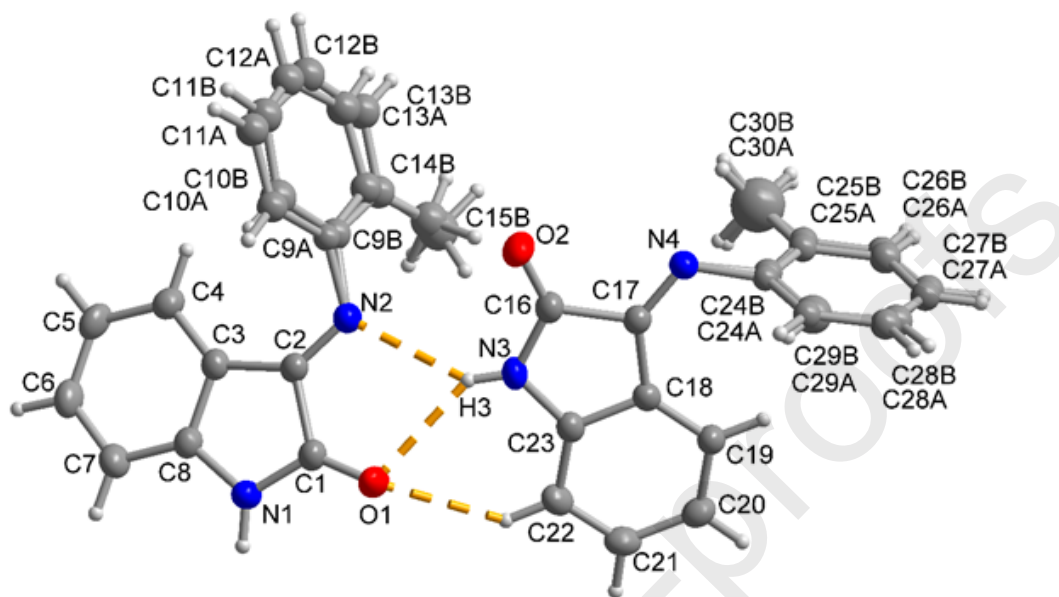


Fig. 1. Molecular structures within the crystal of HL1, showing two symmetry-independent molecules (A and B) in the asymmetric unit, and the hydrogen-bonding interactions between A and B.

Table 2. Some selected bond lengths (Å) and angles (°) in HL1.

Bond lengths (Å)/angles (°)	Molecule A (HL1) (exptl.)	Bond lengths (Å)/angles (°)	Molecule B (HL1) (exptl.)	HL1 (cal.) ¹	HL2 (cal.) ¹	1 (cal.) ²	2 (cal.) ²
C1-O1	1.2114(25)	C16-O2	1.2161(26)	1.2423	1.2422	1.2869	1.2864
C1-N1	1.3619(21)	C16-N3	1.3554(22)	1.4001	1.4006	1.3038	1.3043
C8-N1	1.4127(28)	C23-N3	1.4092(27)	1.4114	1.4107	1.4115	1.4081
C1-C2	1.5303(27)	C16-C17	1.5198(28)	1.5392	1.5395	1.5424	1.5458
C2-N2	1.2762(20)	C17-N4	1.2729(20)	1.2925	1.2935	1.2921	1.2949
N2-C9A/C9B	1.4136(57)/1.4672(60)	N4-C24A/C24B	1.4038(50)/1.4728(71)	1.4125	1.4121	1.4286	1.4170
Zn-O1/O1'						1.9398	1.9398
Zn-N2/N2'						2.0637	2.0637
C2-N2-C9A/C9B	117.74/119.85	C17-N4-C24A/C24B	119.07/117.58	127.78	127.62	123.07	126.49
N2-Zn-N2'						120.15	126.68
O1-Zn-O1'						127.49	131.22
O1-Zn-N2'/N2-Zn-O1'						119.72	115.15
N2-Zn-O1/N2'-Zn-O1'						86.88	86.88
$\theta_1 / ^\circ$ ^a	69.91/70.01		88.10/86.51	57.12	54.38	69.95	48.12
$\theta / ^\circ$ ^b						86.56	77.66

¹ Calculated from optimized structure at B3LYP/LANL2DZ [15];

² Calculated from optimized structure at B3LYP/6-31G(d) for Δ -Zn isomer;

^a $\theta_i/^\circ$ = Angles between the two planes of the aryl- and lactam-rings.

^b $\theta/^\circ$ = Dihedral angles between the two planes formed by the chelating donor atoms with the metal ion (i.e., O1-Zn-N2 and O1'-Zn-N2').

Packing analyses for HL1 explore some intermolecular hydrogen bonding interactions and C–H \cdots π contacts, a common feature found in the isatin-Schiff bases at solid state [14,23,24, 25]. There are three hydrogen bonding interactions between the H3(N3) and O1 [H3–O1 2.37 Å] {or H1(N1) and O2ⁱ [H1–O2ⁱ 2.41 Å]}, H3(N3) and N2 [H3–N2 2.38 Å] {or H1(N1) and N4ⁱ [H1–N4ⁱ 2.35 Å]} and H22(C22) and O1 [H22–O1 2.48 Å] {or H7(C7) and O2ⁱ [H7–O2ⁱ 2.44 Å]}, respectively. Details of the hydrogen bonds are given in Tables 3 (Fig.1). Packing in the crystals, in addition to the hydrogen bonds, is further organized by a few C–H \cdots π contacts [26], whereas there are no π – π contacts [27] even in the presences of extended aromatic rings. Thus, there are a few *intra*- and *inter*-molecular C–H \cdots π contacts, respectively in the crystals (Figs. 2, S6 and Table S1).

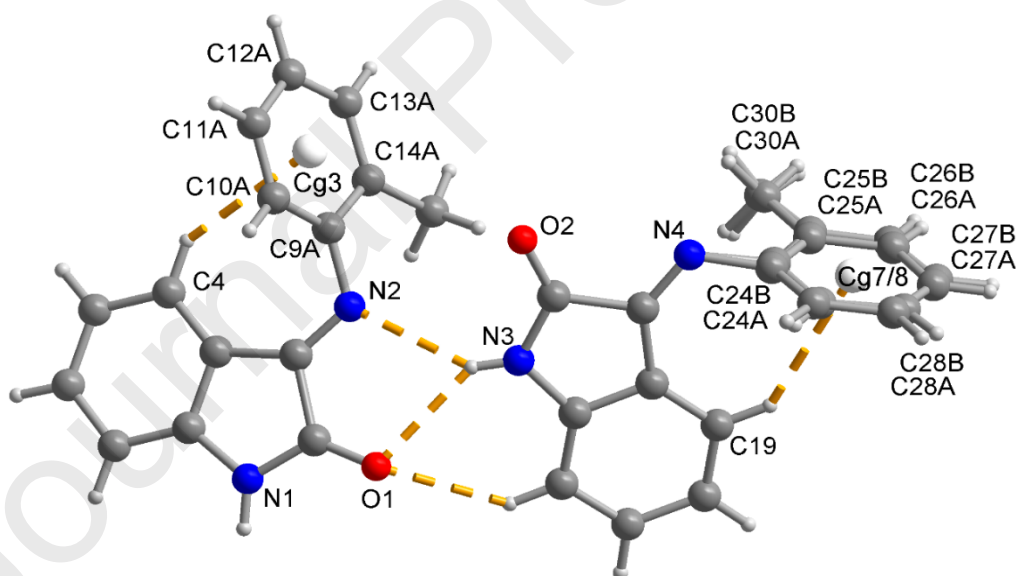


Fig. 2. *Intramolecular* C–H \cdots π contacts along with N–H \cdots O and C–H \cdots O hydrogen bonding (as dashed orange lines) in HL1. Details of these contacts are given in Tables S1 (Cg = ring centroid).

Table 3. Hydrogen bonding parameters in HL1

$D-H\cdots A$	$D-H$ (Å)	$H\cdots A$ (Å)	$D\cdots A$ (Å)	$D-H\cdots A$ (°)
N3—H3 \cdots O1	0.81 (3)	2.37 (2)	3.046 (2)	141 (2)
N3—H3 \cdots N2	0.81 (3)	2.38 (3)	3.064 (2)	143 (2)
N1—H1 \cdots O2 ⁱ	0.88 (2)	2.41 (2)	3.135 (2)	140 (2)
N1—H1 \cdots N4 ⁱ	0.88 (2)	2.35 (2)	3.123 (2)	147 (2)
C7—H7 \cdots O2 ⁱ	0.95	2.44	3.201 (2)	136
C22—H22 \cdots O1	0.95	2.48	3.221 (3)	135

Symmetry code: (i) $x-1/2, -y+1/2, z-1/2$.

3.3. Hirshfeld surfaces analyses

Studies of Hirshfeld surface using the CrystalExplorer [28] strongly support the quantitative analyses of the intermolecular interactions and contacts resulting from supramolecular packing in the crystals [29]. Indeed, the graphical presentation of the Hirshfeld surface with 2D fingerprint plot (Fig. 3a) is an overlay of different contributions resulting from close interactions in the crystals. The plot illustrates O \cdots H and N \cdots H hydrogen bonds as two sharp tails pointing to the lower left, respectively. The upper sharp one represents to the H-bond donor and lower one to the acceptor [2b]. The plot, in addition, reveals two wings at lower middle position for C—H \cdots π contacts. Hirshfeld surface mapped with d_{norm} property (Fig. 3b) [2c] clearly shows the hydrogen bonding interactions and C—H \cdots π contacts as discussed in packing analyses above. The red circles represent the closest contacts (i.e., shorter than the Van der Waals contact), while blue represent the most distant contacts (i.e., longer than the Van der Waals contact) on the d_{norm} surface (Fig. 3b). Breakdown of the Hirshfeld surfaces (fingerprint plot and d_{norm} property) into the contributions from C \cdots C ($\pi\cdots\pi$, 1.0%), C \cdots H (C—H $\cdots\pi$, 31.3%), O \cdots H (10.8%), N \cdots H (4.6%) and H \cdots H (50.4%) interactions, respectively are shown Fig. S7.

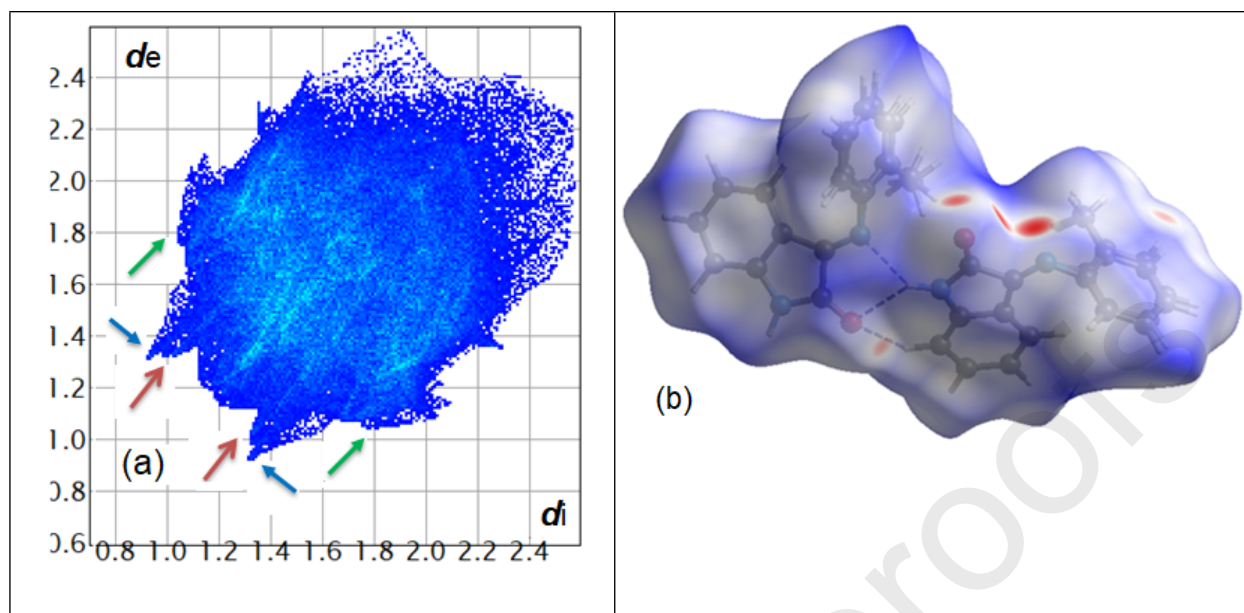


Fig. 3 (a) Graphical presentation of the Hirshfeld surface with 2D fingerprint plot with characteristic features due to C–H...O (red arrows), C–H...N (blue arrows) and C–H... π (green arrows) interactions (d_i and d_e are the distances from the surface to the nearest atom interior and exterior to the surface, respectively), (b) Hirshfeld surface mapped with d_{norm} property (the red spots represent the closest contacts and blue the most distant interactions).

3.4. DFT optimized structures

The optimized structures at B3LYP/6-31G(d) (Fig. 4) demonstrate both the Δ -Zn and Λ -Zn configured isomers are of equi-energetic for **1** or **2**. However, compound **2** is relatively stable than **1** by *ca.* 2.12 Kcal/mol due to less steric hindrance experienced by the *p*-tolyl group in the co-ordination sphere. The calculated bond lengths and angles for **1** or **2** and isatin-Schiff bases (HL1 or HL2) are comparable to the X-ray values for HL1 with the lactam-form (Table 2). The angles (θ_1 /°) between the two planes of the aryl- and lactam-rings are significantly smaller (i.e., 57.1/54.4 ° in HL1/HL2 or 69.95/48.12 in **1/2**) in compare to the X-ray values in HL1 (i.e., *ca.* 69.9/70.0 ° in A or *ca.* 88.1/86.5 ° in B) due to the presence of intermolecular hydrogen bonds and C–H... π contacts in the crystal, as mentioned above [14]. These interactions are obviously absent in the optimization structures at gas phase. The interactions in the crystal packing squeeze the bond angles C2-N2-C9A/C9B (*ca.* 117.7/119.9 ° in A) and C17-N4-C24A/C24B (*ca.* 119.1/117.6 ° in B) in comparison to those of the calculated values (*ca.* 127.8/127.6 ° in

HL1/HL2 or *ca.* 123.1/126.5 ° in **1/2**). However, the dihedral angles ($\theta/^\circ$) between two planes formed by the chelating donor atoms with the metal ion (i.e., planes O1-Zn-N2 and O1'-Zn-N2') provide quantitative measure of the geometry for the complexes [4,6,11,12]. Thus, the dihedral angles ($\theta/^\circ$) values of 86.6 ° (**1**) and 77.7 ° (**2**) explore the distorted tetrahedral geometry for the complexes.

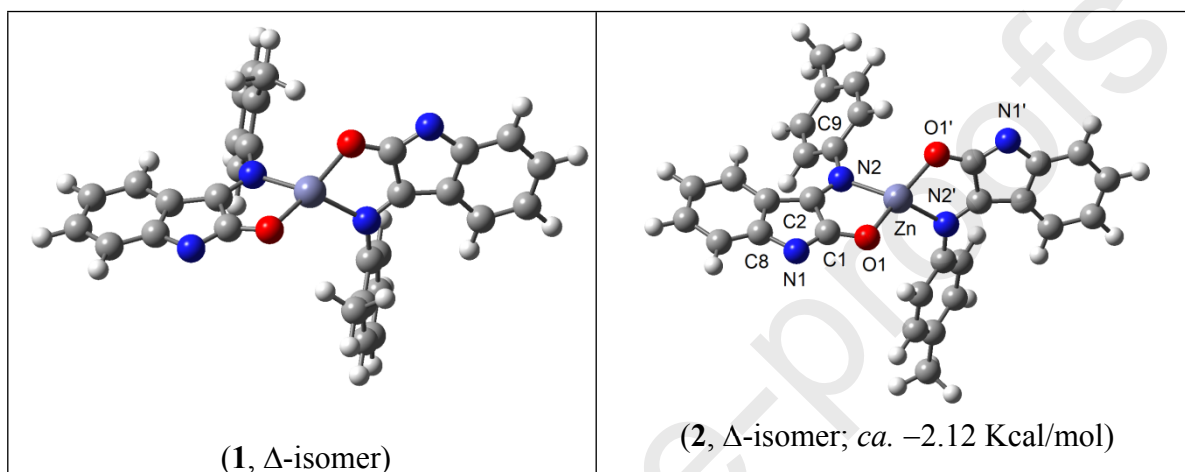


Fig. 4. DFT optimized structures for **1** and **2**, calculated at B3LYP/6-31G(d), respectively.

3.5. Electronic and computed spectra

Electronic spectra for the isatin-Schiff bases and their complexes in methanol are identical (Fig. 5), and feature strong bands below 340 nm with absorption maxima (λ_{\max}) at 248 nm $\{\epsilon = 21629$ (HL1), $34035 \text{ dm}^3 \text{ mol}^{-1} \text{ cm}^{-1}$ (**2**) $\}$ and at 292 nm $\{\epsilon = 4462$ (HL1), $7079 \text{ dm}^3 \text{ mol}^{-1} \text{ cm}^{-1}$ (**2**) $\}$ due to the intra-ligand $\pi \rightarrow \pi^*$ and $n \rightarrow \pi^*$ (LL) transitions, respectively [3,6-7,9,13]. The relatively weak broad band at 350-500 nm with absorption maximum at 414 nm $\{\epsilon = 2552$ (HL1), $4257 \text{ dm}^3 \text{ mol}^{-1} \text{ cm}^{-1}$ (**2**) $\}$ is attributed to the intra-ligand charge transfer (LLCT) transitions. The excited state properties by TDDFT using different combinations of the functionals and the basis sets, respectively, provide identical electronic spectra (Fig. S4). These results strongly support the reliability and validity of the methods employed as well as the electronic properties of the complex. However, the calculated electronic spectra are comparable to the experimental one with little shifting of the band maxima (Fig. 5 and Table 4). Indeed, the spectra for Δ -Zn and Λ -Zn configured isomers are essentially identical (Fig. S5).

A few selected and simplified assignments on the computed spectra are made based on the molecular orbitals (MOs) and population analyses and compared to the experimental data (Table 4). A combined band resulting from MM, ML and LL transitions is found at 481 nm, close to the experimental band at *ca.* 414 nm, for HOMO to LUMO+1 and HOMO-1 to LUMO transitions with MOs contributions of 49 and 48 %, respectively (Fig. 6 and Table 2). The HOMO, LUMO and LUMO+1 orbitals are mainly localized on the π -electrons clouds of both the lactam- and aryl-ring, while the HOMO-1 is localized on the π -electrons clouds of the lactam-ring only (Fig. 6). Although the metal d-d electrons transitions, for the present diamagnetic closed shell Zn-complex, are not allowed, however, there are a bit of d-electrons clouds in the HOMO/HOMO-1. This is because the metal-d MO has same symmetry as the ligand MOs, provides a very small degree of electrons clouds to the metal-d MO (Fig. 6). Indeed, a very insignificant d-electrons clouds in the LUMO/LUMO+1 represent a tiny bit of back donation again due to same symmetry of the metal-d MO and ligand MOs. As a result, excited state properties potentially provide a very little d-d contributions in addition to the ligand centred π -transitions (Fig. 6 and Table 4).

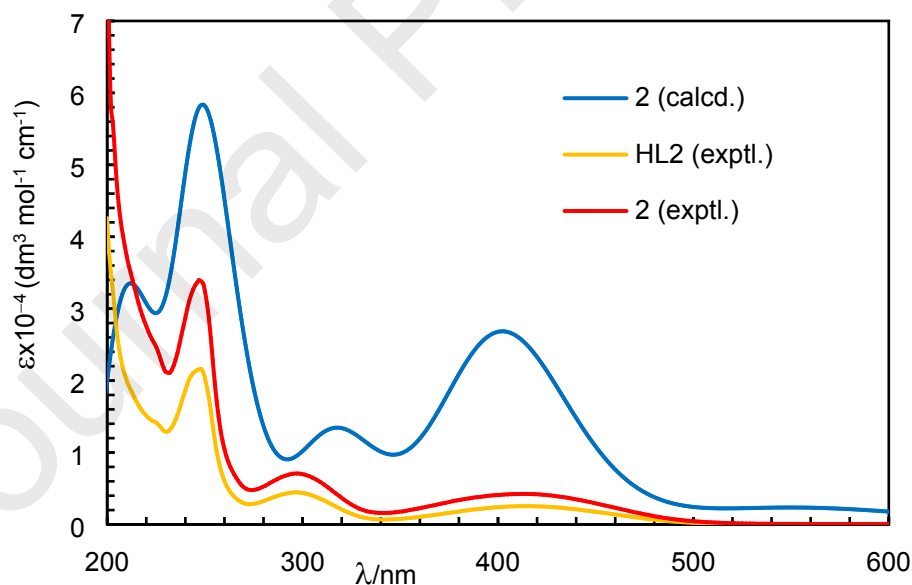


Figure 5. UV-Vis. spectra for HL2 (0.015 mmol/L) and **2** (0.08 mmol/L) in MeOH at 25 °C, and calculated spectrum for **2** (Δ -Zn isomer) at b3lyp/tzvp//b3lyp/6-31g(d) in methanol using PCM.

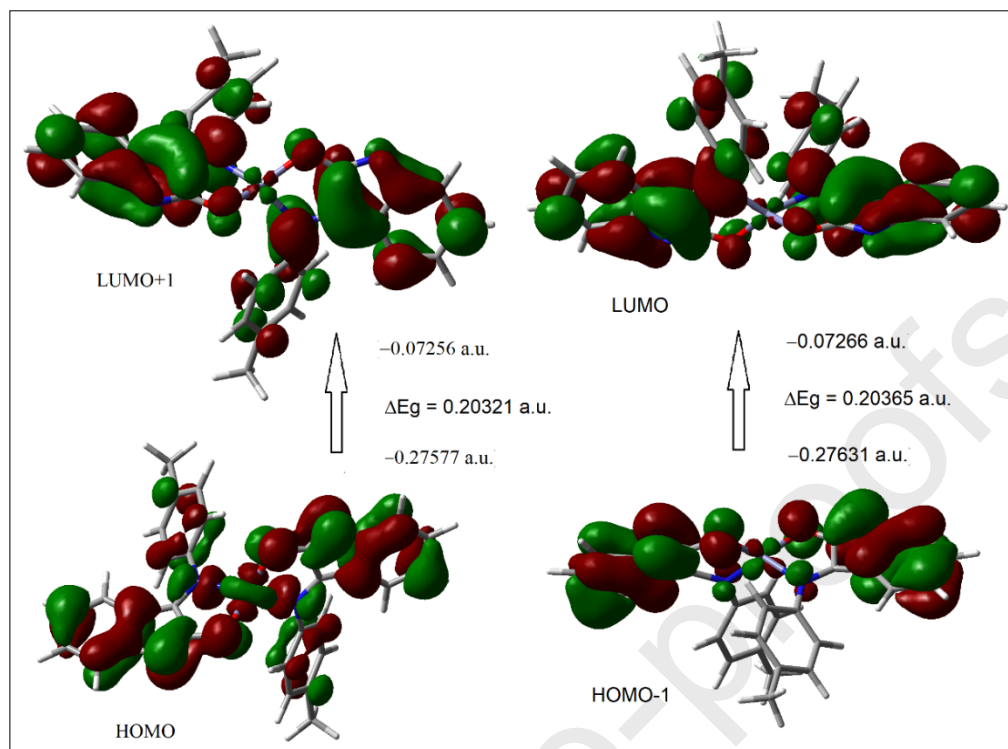


Fig. 6. Frontier molecular orbitals (HOMO, HOMO-1, LUMO, and LUMO+1) for **2** (Δ -Zn isomer), calculated at b3lyp/tzvp//b3lyp/6-31g(d) in methanol (Isovalue 0.02).

Table 4.

Assignments on calculated spectra for **2** (Δ -isomer) at b3lyp/tzvp//b3lyp/6-31g(d) in methanol using PCM.

λ_{\max}/nm ¹	Oscillator strength (f)	MOs contributions (%) ²	Assignments ³
481 (414)	0.0406	H \rightarrow L+1 (49), H-1 \rightarrow L (48)	MM, ML, LL
348	0.4517	H-3 \rightarrow L (38), H-2 \rightarrow L+1 (49)	MM, ML, LL
314 (292)	0.0944	H-9 \rightarrow L (39), H-8 \rightarrow L+1 (47)	MM, ML, LL
249 (248)	0.3340	H-13 \rightarrow L+1 (25), H-10 \rightarrow L (35)	MM, ML, LL
235	1.1001	H-11 \rightarrow L+1 (14), H-1 \rightarrow L+5 (14)	ML, LL
205	0.2593	H-3 \rightarrow L+7 (9), H-2 \rightarrow L+4 (24)	ML, LL

¹ Experimental values are in parentheses; ² H = HOMO and L = LUMO; ³ MM = metal-centered (d-d), ML = metal-ligand, LL = ligand-centered transitions bands.

3.6. Lactam (L)- and Enol (E)-tautomers

^1H NMR spectrum of HL2 is shown in Fig. 7, and spectral data are summarized in the experimental section. The isatin-Schiff bases undergo a dynamic tautomerization between the lactam (L)- and enol (E)-forms (Scheme 1) and show peaks for both the forms simultaneously in solution. The ratio of lactam- to enol-form varies with time as evidenced by variable time ^1H NMR studies in solution [14-15]. Thus, the methyl protons show two singlets at δ 2.18 (*ca.* 90%) and 2.38 (*ca.* 10%) ppm in HL1 and at 2.43 (*ca.* 85%) and 2.28 (*ca.* 15%) ppm in HL2, correspond to the lactam- and enol-forms, respectively. The phenolic O-H (enol-form) and amine N-H (lactam-form) protons show broad signals at δ 9.35 and 9.63 ppm in HL1 and 8.91 and 9.19 ppm in HL2, respectively (Fig. 7). In accordance with the solid-state X-ray structure for HL1 with lactam-form (discussed above), we assume the major tautomer to be the lactam-form and the minor one to be the enol-form immediately upon dissolution. Peak assignments and their percentages are made based on the peak integration values for the methyl and N-H (Lactam)/O-H (Enol) protons, respectively. The results are in good accord with the vibrational studies showing both forms in solution, as discussed above.

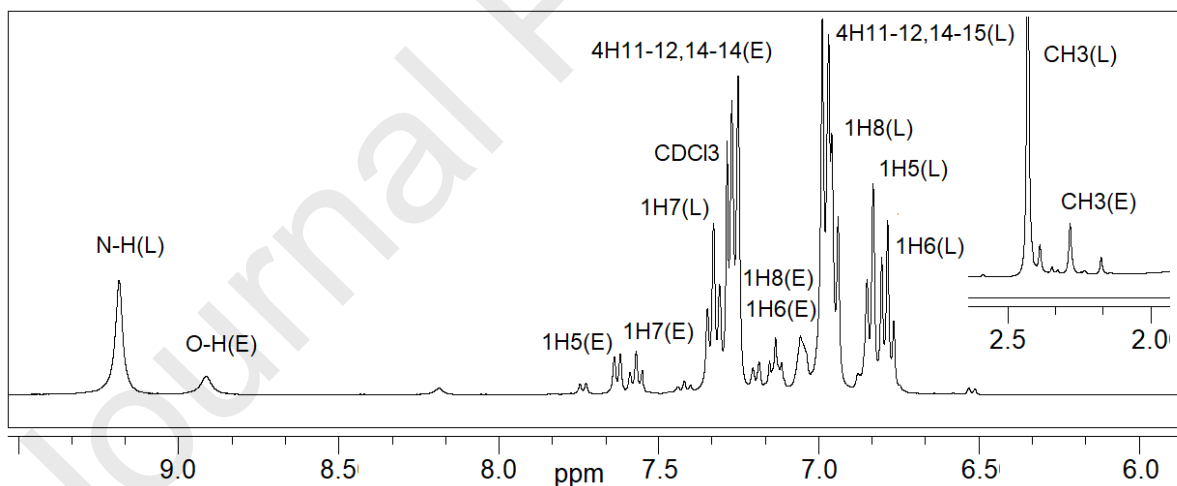


Fig. 7. ^1H NMR spectrum of the 3-(*p*-tolylimino)indolin-2-one (HL2) in CDCl_3 at 20 °C (L and E represent the lactam- and enol-forms, respectively).

3.7. Δ -Zn and Λ -Zn isomers

^1H NMR spectra for **1** and **2** in CDCl_3 (Fig. 8) show the peaks associated to the co-ordinated Schiff bases ligands to the metal ion. As mentioned above, the enol-form of ligands reacts with the metal ion *via* deprotonation of the enolic proton and forms the complexes in solution (Scheme1). Thus, the broad peaks found for N-*H* (lactam) and O-*H* (enol) protons (i.e., at δ 9.63/9.35 ppm in HL1 or 9.19/8.91 ppm in HL2, Fig. 7) are absent in the spectra (Fig. 8). Rather, the spectra show two sets of peaks for each proton in accordance with the existences of the two possible Δ -Zn and Λ -Zn configured isomers with a ratio of *ca.* 65:35 (Δ : Λ or Λ : Δ). The amounts of the isomers were calculated based on integration values of the most downfield aromatic peaks, respectively. Labelling of the peaks as Δ - or Λ -isomer may be in reversed way. Indeed, spectra taken at different time intervals show no significant changes of this ratio within 45 min, 4 h and 24 h of complex dissolution in CDCl_3 , respectively. Hence, the results rule out any interconversion between the two isomers in solution, that is, same ratio of the isomers (*ca.* 65:35) exists at solid state. Or, a rapid equilibrium between the two isomers has been established immediately upon dissolution, provides a ratio of *ca.* 65:35, irrespective of the ratio at solid state. However, the results indicate preferred formation of the Δ -Zn or Λ -Zn isomer both in solution and at solid state, based on the thermodynamic and/or kinetic stability, as evidenced in the analogous Zn(II)-Schiff bases complexes [3,6-7,9,13]. In fact, comparable results of diastereomers at a ratio of *ca.* 77:23 (Δ : Λ or Λ : Δ) within 10 min, 4 h and 20 h of complex dissolution, respectively were reported for the zinc(II)-(*S*)-naphthaldimine complexes [6]. Thus, ^1H NMR results strongly support the formation of the Δ -Zn and Λ -Zn configured isomers resulting from induced chirality at-metal centre by the N,O-chelate ligands in distorted tetrahedral Zn(II)-isatin Schiff bases complexes.

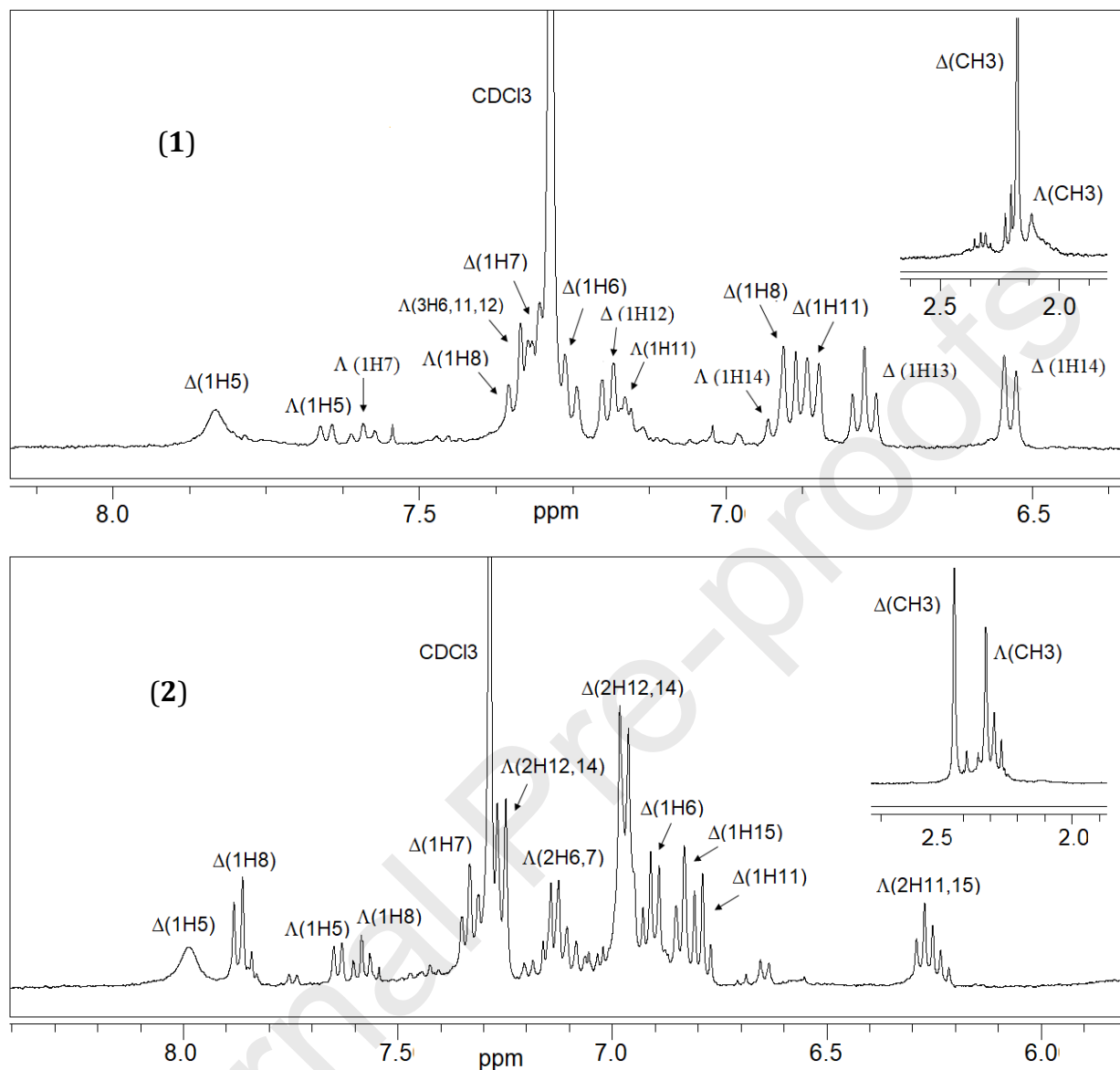


Fig. 8. ^1H NMR spectra of the *bis*[3-(*o/p*-tolylimino)indole-2-olato- $\kappa^2\text{N,O}$]- Δ/Λ -zinc(II) (**1** and **2**) in CDCl_3 at 20 °C (labelling of the peaks as Δ - or Λ -isomer may be in reversed way).

4. Conclusion

The isatin-Schiff bases 3-(*o/p*-tolylimino)indolin-2-one (HL1 and HL2) undergo tautomerization from lactam (L)- to enol (E)-form which in turn reacts with the zinc(II) nitrate to give the *bis*[3-(*o/p*-tolylimino)indole-2-olato- $\kappa^2\text{N,O}$]- Δ/Λ -zinc(II) (**1** and **2**). Vibrational spectra show the bands for $\nu\text{N-H}$ and $\nu\text{O-H}$ (or $\nu\text{C=O}$) in HL1 or HL2, which are absent in **1** or **2**, indicate the formation of the complexes. Spectra for HL1 or HL2 show solely the lactam-form at solid state, while both forms in solution. ^1H NMR studies reveal both the lactam- and enol-tautomers in solution.

Molecular structure determination for HL1 explore two symmetry independent molecules (A and B) in an asymmetric unit due to intermolecular hydrogen-bonding interactions and C-H... π contacts. Studies of Hirshfeld surfaces using the CrystalExplorer strongly support quantitative analyses by supramolecular packing in the crystals. ^1H NMR spectra indicate formation of the Δ -Zn and Λ -Zn configured isomers (with one preferential formation) resulting from induced chirality at-metal centre in **1** or **2**. Optimized structures and excited state properties by DFT/TDDFT correspond well to the experimental results.

Declaration of interests

The authors declare that they have no known competing financial interests or personal relationships that could have appeared to influence the work reported in this paper.

The authors declare the following financial interests/personal relationships which may be considered as potential competing interests:

Declaration of interests "None"

On behalf of all authors



Mohammed Enamullah

Acknowledgement

We acknowledge Wazed Miah Science Research Centre (WMSRC) at Jahangirnagar University, Bangladesh for obtaining elemental and H NMR data. Our sincere thanks to Professor ABP Lever, Department of Chemistry, York University, Toronto for many useful discussions on spectral analyses by DFT/TDDFT and the [computecanada.ca](https://ccdb.computecanada.ca/) (<https://ccdb.computecanada.ca/>) Ontario, Canada for using their computational resources.

References

- [1] (a) A. von Zelewsky, *Stereochemistry of Coordination Compounds*, John Wiley & Sons, Chichester (1996) 69; (b) H. Amouri, M. Gruselle, *Chirality in Transition Metal Chemistry: Molecules, supramolecular assemblies and materials*, John Wiley & Sons, Chichester (2008) 40; (c) K.A. Jensen, *Inorg. Chem.* 9 (1970) 1; (d) R.E. Ernst, M.J. O'Connor, R.H. Holm, *J. Am. Chem. Soc.* 89 (1967) 6104; (e) R.S. Downing, F.L. Urbach, *J. Am. Chem. Soc.* 91 (1969) 5977; (f) A.-C. Chamayou, S. Lüdeke, V. Brecht, T. B. Freedman, L. A. Nafie, C. Janiak, *Inorg. Chem.* 50 (2011) 11363; (g) A.-C. Chamayou, G. Makhloufi, L.A. Nafie, C. Janiak, S. Lüdeke, *Inorg. Chem.* 54 (2015) 2193.
- [2] (a) C. Evans, D. Luneau, *J. Chem. Soc. Dalton Trans.* (2002) 83; (b) H. Sakiyama, H. Okawa, N. Matsumoto, S. Kida, *Bull. Chem. Soc. Jpn.* 64 (1991) 2644; (c) H. Sakiyama, H. Okawa, N. Matsumoto, S. Kida, *J. Chem. Soc. Dalton Trans.* (1990) 2935; (d) H. Ōkawa, M. Nakamura, S. Kida, *Inorg. Chim. Acta* 120 (1986) 185; (e) T. Akitsu, Y. Einaga, *Polyhedron* 24 (2005) 2933; (f) T. Akitsu, Y. Einaga, *Polyhedron* 24 (2005) 1869; (g) T. Akitsu, Y. Einaga, *Acta Crystallogr. C*, 60 (2004) m640.
- [3] M. Enamullah, V. Vasylyeva, C. Janiak. *Inorg. Chim. Acta* 408 (2013) 109.
- [4] M. Enamullah, M.K. Islam, *J. Coord. Chem.* 66 (2013) 4107.
- [5] M. Enamullah, A.K.M. Royhan Uddin, G. Pescitelli, R. Berardozzi, G. Makhloufi, V. Vasylyeva, A.-C. Chamayou, C. Janiak, *Dalton Trans.* 43 (2014) 3313.
- [6] M. Enamullah, G. Makhloufi, R. Ahmed, B. Alif Joy, M.A. Islam, D. Padula, H. Hunter, G. Pescitelli, C. Janiak. *Inorg. Chem.* 55 (2016) 6449.
- [7] M. Enamullah, M.A. Quddus, M.A. Halim, M.K. Islam, V. Vasylyeva, C. Janiak, *Inorg. Chim. Acta* 427 (2015) 103.

- [8] M. Enamullah, M.A. Islam, B.A. Joy, G.J. Reiss, *Inorg. Chim. Acta* 453 (2016) 202.
- [9] M. Enamullah, V. Vasylyeva, M.A. Quddus, M.K. Islam, S.-P. Höfert, C. Janiak, *CrystEngComm*. 20:33 (2018) 4724.
- [10] M. Enamullah, M.A. Quddus, M.R. Hasan, G. Pescitelli, R. Berardozzi, G.J. Reiß, C. Janiak, *Eur. J. Inorg. Chem.* 2758 (2015).
- [11] G. Pescitelli, S. Lüdeke, A.-C. Chamayou, M. Marolt, V. Justus, M. Górecki, L. Arrico, L. Di Bari, M.A. Islam, I. Gruber, M. Enamullah, C. Janiak, *Inorg. Chem.* 57 (2018) 13397.
- [12] M. Enamullah, M.A. Quddus, M.R. Hasan, G. Pescitelli, R. Berardozzi, G. Makhloufi, V. Vasylyeva, C. Janiak, *Dalton Trans.* 45 (2016) 667.
- [13] M. Enamullah, M.A. Islam, B.A. Joy, B. Dittrich, G.J. Reiss, C. Janiak. *Inorg. Chim. Acta* 482 (2018) 935.
- [14] M. Enamullah, A.K.M. Royhan Uddin, G. Hogarth. *J. Coord. Chem.* 65 (2012) 4263.
- [15] M. Enamullah, M.Al-M. Zaman, M.M. Bindu, M.K. Islam, M.A. Islam, *J. Mol. Struct.* 1201 (2020) 127207.
- [16] APEX2, data collection program for the CCD area-detector system, Version 2.1-0, Bruker Analytical X-ray Systems: Madison (WI) (2006).
- [17] SAINT, data reduction and frame integration program for the CCD area-detector system, Bruker Analytical X-ray Systems: Madison (WI) (2006).
- [18] G. Sheldrick, *Acta Cryst. A* 64 (2008) 112.
- [19] G.M. Sheldrick, Program SADABS, University of Göttingen: Göttingen, Germany (1996).
- [20] K. Brandenburg, Diamond (Version 3.2), Crystal and Molecular Structure Visualization, Crystal Impact – K. Brandenburg & H. Putz Gbr: Bonn, Germany (2009).
- [21] Gaussian 09, Revision D.01, M.J. Frisch, G.W. Trucks, H.B. Schlegel, G.E. Scuseria, M.A. Robb, J.R. Cheeseman, G. Scalmani, V. Barone, B. Mennucci, G.A. Petersson, H. Nakatsuji, M. Caricato, X. Li, H.P. Hratchian, A.F. Izmaylov, J. Bloino, G. Zheng, J.L. Sonnenberg, M. Hada, M. Ehara, K. Toyota, R. Fukuda, J. Hasegawa, M. Ishida, T. Nakajima, Y. Honda, O. Kitao, H. Nakai, T. Vreven, J.A. Montgomery, Jr., J.E. Peralta, F. Ogliaro, M. Bearpark, J.J. Heyd, E. Brothers, K.N. Kudin, V.N. Staroverov, R. Kobayashi, J. Normand, K. Raghavachari, A. Rendell, J.C. Burant, S.S. Iyengar, J. Tomasi, M. Cossi, N. Rega, J.M. Millam, M. Klene, J.E. Knox, J.B. Cross, V. Bakken, C. Adamo, J. Jaramillo, R. Gomperts, R.E. Stratmann, O. Yazyev, A.J. Austin, R. Cammi, C. Pomelli,

- [22] T. Bruhn, A. Schaumlöffel, Y. Hemberger, G. Bringmann. *Chirality* 25 (2013) 243.
- [23] (a) M. Akkurt, S. Ozturk, A. Ercag, M.U. Ozgur, F. W. Heinemann. *Acta Cryst.* E59 (2003) o780;(b) A. Ercag, S.O. Yildirim, M. Akkurt, M.U. Ozgur, F.W. Heinemann. *Chin. Chem. Lett.* 17 (2006) 243;(c) Y-F. Sun, J-K. Li, Z-B. Zheng. *Acta Crystallogr.* E63 (2007) o2520;(d) S. Ozturk, M. Akkurt, M.U. Ozgur, A. Ercag, F.W. Heinemann. *Acta Cryst.* E59 (2003) o569;(e) M.C. Rodriguez-Arguelles, M.B. Ferrari, F. Bisceglie, C. Pelizzi, G. Pelosi, S. Pinelli, M. Sassi. *J. Inorg. Biochem.* 98 (2004) 313.
- [24] (a) G. Pelosi, M.B. Ferrari, M.C. Rodriguez-Arguelles, S. Mosquera-Vazquez, J. Sanmartin. *Acta Cryst.* C62 (2006) m241; (b) G. Pelosi, C. Pelizzi, M.B. Ferrari, M.C. Rodriguez-Arguelles, C. Vieito, J. Sanmartin. *Acta Cryst.* C61 (2005) o589; (c) J.S. Casas, A. Castineiras, M.C. Rodriguez-Arguelles, A. Sanchez, J. Sordo, A. Vazquez-Lopez, E. Vazquez-Lopez. *J. Chem. Soc. Dalton Trans.* (2000) 4056.
- [25] (a) X. Zhong, H-L. Wei, W-S. Liu, D-Q. Wang, X. Wang. *Bioorg. Med. Chem. Lett.* 17 (2007) 3774;(b) A. Coda, G. Gatti, A.C. Coda, G. Desimoni, P.P. Righetti, G. Tacconi. *Gazz. Chim. Ital.* 115 (1985) 549;(c) H.M. Ali, S.N.A. Halim, S.W. Ng. *Acta Cryst.* E61 (2005) o3287;(d) H.M. Ali, M. Laila, M.R. Rizal, S.W. Ng. *Acta Cryst.* E64 (2008) o921;(e) H.M. Ali, S.N.A. Halim. S.W. Ng, *Acta Cryst.* E61 (2005) o916.
- [26] (a) M. Nishio, *Phys. Chem. Chem. Phys.* 13 (2011) 13873; (b) M. Nishio, Y. Umezawa, K. Honda, S. Tsuboyama, H. Suezawa, *CrystEngComm.* 11 (2009) 1757; (c) M. Nishio, *CrystEngComm.* 6 (2004) 130; (d) C. Janiak, S. Temizdemir, S. Dechert, W. Deck, F. Girgsdies, J. Heinze, M.J. Kolm, T.G. Scharmann, O.M. Zipffel, *Eur. J. Inorg. Chem.* (2000) 1229; (e) Y. Umezawa, S. Tsuboyama, K. Honda, J. Uzawa, M. Nishio, *Bull. Chem. Soc. Jpn.* 71 (1998) 1207; (f) M. Nishio, M. Hirota, Y. Umezawa, *The CH/ π interaction (evidence, nature and consequences)*, Wiley-VCH, New York (1998).
- [27] (a) X.-J. Yang, F. Drepper, B. Wu, W.-H. Sun, W. Haehnel and C. Janiak, *Dalton Trans.* (2005) 256 and Supplementary Material therein; (b) C. Janiak, *J. Chem. Soc. Dalton Trans.*, (2000) 3885.

J.W. Ochterski, R.L. Martin, K. Morokuma, V.G. Zakrzewski, G.A. Voth, P. Salvador, J.J. Dannenberg, S. Dapprich, A.D. Daniels, Ö. Farkas, J.B. Foresman, J. V. Ortiz, J. Cioslowski, D.J. Fox, Gaussian, Inc., Wallingford CT, 2009.

-
- [28] (a) CrystalExplorer17, Version 17.5; (b) M.J. Turner, J.J. McKinnon, S.K. Wolff, D.J. Grimwood, P.R. Spackman, D. Jayatilaka, M.A. Spackman, © 2005-2017 University of Western Australia, 2017. <http://hirshfeldsurface.net>
- [29] (a) J.J. McKinnon, M.A. Spackman, A.S. Mitchell, *Acta Cryst. B*60 (2004) 627; (b) M.A. Spackman, J.J. McKinnon, *CrystEngComm*. 4 (2002) 378; (c) J.J. McKinnon, D. Jayatilaka, M.A. Spackman, *Chem. Commun.* (2007) 3814.